Clogging of microporous channels networks: role of connectivity and tortuosity

Patrice Bacchin · Quentin Derekx · Damien Veyret · Karl Glucina · Philippe Moulin

Abstract The aim of this work is to study the pore blocking by the use of microfluidic devices (microseparators) and numerical simulation approaches. The microseparators are made in PDMS and are constituted of an array of microchannels 20 μm wide with three types of structure: straight microchannels, connected microchannels (or aligned square pillars) and staggered square pillars in order to mimic merely the complexity of the flow encountered in filters or membranes (tortuosity, connectivity between pores). Direct observation with video microscopy of filtrations of 5 μm latex particles has been performed to examine the capture of particles. The results show a piling up of particles within the porous media leading to a clogging. The capture efficiency remains low (<0.1 %). In the case of filtration in the forest of pillars, the capture is faster and arises mainly between the pillars. The increase in tortuosity in the microseparator leads then to a rise of the clogging. It must be caused by the increase in critical trajectories leading to the capture of particles on the PDMS walls. At the same time, numerical simulations of filtration in parallel with microchannels have been performed in the same flow conditions with GeoDict software. The different kind of experimental deposit structure can be simulated, but there is still inaccuracy in the description of the accumulation kinetics. These discrepancies are probably due to the lack of accuracy to depict particle/particle colloidal interactions in simulations and the fact that re-suspension of particles after capture is not well described.

Keywords Microchannels · Plugging · Filtration · Numerical simulation · Fouling

P. Bacchin (✉) · Q. Derekx
Laboratoire de Génie Chimique, INPT, UPS, Université de Toulouse, 118 Route de Narbonne, 31062 Toulouse, France
e-mail: bacchin@chimie.ups-tlse.fr

Q. Derekx
e-mail: derekx@chimie.ups-tlse.fr

P. Bacchin · Q. Derekx
CNRS, UMR 5503, 31062 Toulouse, France

Q. Derekx
Laboratoire de Mécanique, Modélisation et Procédés Propres (CNRS UMR 6181), Aix Marseille Université, Europôle de l'Arbois BP80, Bâtiment Laënnec, 13545 Aix-en-Provence Cedex 04, France

Q. Derekx · P. Moulin
CNRS, UMR 7340, 13545 Aix en Provence, France
e-mail: philippe.moulin@univ-cezanne.fr

D. Veyret
Technopôle de Château-Gombert, Polytech Marseille (CNRS UMR 6595), 5 rue Enrico Fermi, 13453 Marseille Cedex 3, France
e-mail: damien.veyret@laposte.net

K. Glucina
Pôle Eau Potable, Suez Environnement, CIRSEE, 38, rue du Président Wilson, 78230 Le Pecq, France
e-mail: karl.glucina@suez-env.com

1 Introduction

The understanding of pore clogging is an important scientific challenge to maintain flow in microfluidic systems transporting particles as well as to optimize the efficiency of processes. For instance, the prediction of internal clogging in membrane processes is still impossible in the water treatment. The understanding of the conditions under which particles clog a porous media and the reversibility of the capture process (by a flow reversal, a

phase change, etc) is a scientific challenge with important technical consequences.

Nowadays, it is impossible to know how the particles are captured by the membrane mainly because of the complex interplay between the particle–membrane interactions and the hydrodynamics occurring at pore scale in this process (Bacchin et al. 2011; Bowen et al. 1999; Kim and Zydney 2004). The interplay between surface interactions and hydrodynamics gives rise to interesting possibilities to limit the fouling that has been investigated via the critical flux concept (Bacchin et al. 2006a): a flux below which fouling is limited because of surface interactions that overcome drag force pushing particles toward the membrane. The critical flux concept has shown its relevance to understand how the dispersion stability combines to the filtration conditions and leads to very different fouling scenarios. However, a sharp transition between a dispersed and a solid phase is not often observed in practice, and discrepancies between the models and experiments still exist (Bacchin et al. 2006b), even with well characterized suspensions and membranes. One possible cause for these discrepancies is the fact that such membrane cannot be represented as a continuous porous surface with homogeneous properties, an assumption often done in simulations. Phenomena occurring at pore scale like pore clogging are then of importance: experimental and theoretical studies are needed to progress in their understanding.

In the last decades, different experimental studies have brought into light the importance of the pore scale on the fouling phenomena. A key has been the experimental development of new in situ quantifications of physical and chemical processes occurring during filtration (Chen et al. 2004) often based on microfluidic techniques. Bromley et al. (2002) showed a critical flux fivefold higher with slotted pores than with circular pores. Similarly, Chandler and Zydney (2006) realized a filtration experiment of a yeast cell on slot-shaped or circular pores and demonstrated that the flux decline was slower with slotted pores. In such microsystems when analyzing deposition of latex particles near circular pores, Lin et al. showed the existence of two preferential locations for particle deposition near the pore entrance. All these results clearly indicate the impact of the local structure at the membrane surface on the first step of the clogging phenomena. Furthermore, other experiments (Kuiper et al. 2000) with microsieves with circular pores but various porosities have shown that the latter plays an important role in the development of the cake layer at the membrane surface. For a high porosity, i.e., pores very close to each other, steric hindrance can occur between particles and prevents their deposition over the whole membrane surface. Similar situations were experimentally evidenced by Ramachandran and Fogler (1999, 1998) using direct visualizations of track-etched membranes, at pore scale, after filtration experiments performed with well latex dispersions of well-controlled particle sizes. Their experiences highlighted the formation of particle cluster at the pore entrance. The formation of particle cluster leading to arches in microchannels has been observed and analyzed in channels for a size ratio around 0.3 even for dilute suspensions (Sharp and Adrian 2005). Mustin and Stoeber (2010) also showed that a low concentration of relatively large particles in a suspension has a major effect on the average time for a microchannel to be blocked by particles. In 2012, Agbangla et al. have determined experimentally critical conditions for the formation of arches leading to the formation of deposit at the pore entrance. Critical conditions in terms of a combination of operating conditions (combination of the particle concentration and the particle velocity) have been identified. Such a behavior has been pointed out by (Wyss et al. 2006) the time required to reach channel clogging depends on hydrodynamics; the clogging increases with the flow rate because of the increasing amount of transported colloidal particles. All these studies demonstrate that the 3D structure of the clogging results from the preliminary particle deposition (for example with arches formation) being very dependent on the transport at pore scale.

On a theoretical point of view, a limited number of numerical studies copes with the above-mentioned difficulties, associated with a description of the fouling at pore scale. Bowen et al. (1999) computed the electrostatic interaction between a single charged particle and a pore, modeled as a cylindrical opening in a flat charged plane for various particle positions. They found some equilibrium positions for the particle, located above the pore when the drag force exerted by the particle corrected for pore-particle hydrodynamic interactions is balanced by the repulsive electrostatic interaction. If the fluid velocity exceeds a given critical value, the drag force can overcome the repulsive force and the particle can flow through the pore. However, these approaches have been developed for dilute systems and do not account for multibody interparticle interactions occurring near a pore entrance. More recently, Ando et al. (2012) performed simulations accounting multiple surface interaction between particles at a pore entrance and showed different fouling modes according to the pore/particle size ratio: for a ratio of 3.6, initially particles filled the pores and then form a cake layer on the surface of membrane, whereas when the ratio is lower (2.5), particles are accumulated on the surface of the membrane without filling the pores and a cake layer forms across the entire filtration. These simulations also show the effect of these clogging structures on the efficiency of backwash sequences. Henry et al. (2012) have reviewed the modeling approaches taking into account the competition between particle–fluid, particle–surface and particle–particle interactions existing in pore clogging phenomena. They confirm that, depending on

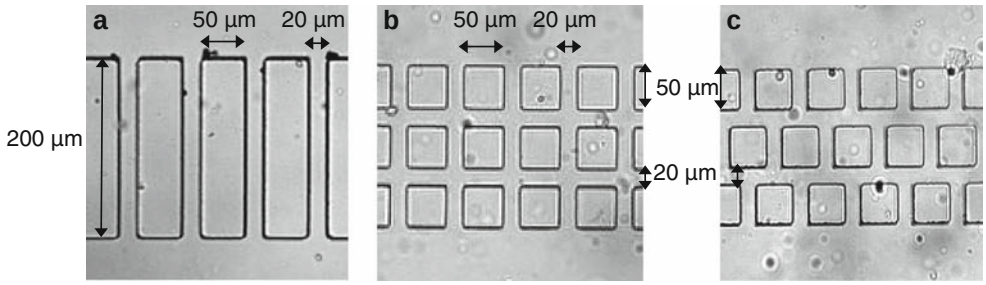

Fig. 1 **a** Straight parallel microchannels, **b** connected microchannels or aligned square pillars **c** staggered square pillars

hydrodynamic conditions (flow velocity), fluid characteristics (such as ionic strength) as well as particle and substrate properties (such as zeta potentials) particle deposition can lead to the formation of either a single monolayer or multilayers and then to very different clogging dynamic.

The results mentioned above highlight the need for studies performed at pore scale, in order to progress toward a better understanding and prediction of clogging and fouling mechanisms. At that point, it is worth mentioning that even if the so-called filtration laws are based on fouling models involving a description at the pore scale, such as complete or intermediate pore blocking, pore section narrowing (Hermia 1982), they are typically used at membrane scale to describe for instance the decline in permeate flux as fouling goes on. Thus, they are not able to properly model situations where membrane heterogeneity is important (Grenier et al. 2008).

Our aim, in this paper, is to investigate the plugging of porous media with an approach coupling microfluidic experiment and pore-scale simulation. In this context, we develop with microfluidic techniques, microseparator devices in PDMS material allowing the direct observation of the internal clogging in microfluidic porous media (Bacchin et al. 2011). In this paper, the filtration results of microseparators with different pore geometries are discussed at the light of numerical simulation.

2 Materials and methods

2.1 PDMS microseparators

We developed polydimethylsiloxane (PDMS) microfluidic devices mimicking pore scale of filtration systems with arrangement of microchannels. Thanks to the transparency of PDMS, these microseparators allow a direct observation of the dynamic of particle clogging under microscope. The PDMS microseparators used in the present study were made by the usual soft lithography technique (McDonald et al. 2000). Three types of structure were designed in the present work: straight microchannels (Fig. 1a), connected microchannels or aligned square pillars (Fig. 1b) and staggered square pillars (Fig. 1c) in order to mimic merely the complexity of the flow encountered in filters or membranes (tortuosity and connectivity between pores). The common depth of all the channels of the network is 50 µm, and the bottleneck size is 20 micrometers. The specific dimensions of each microseparator[2] are specified in Fig. 1.

A schematic view of the design of the whole microseparators has been presented in previous papers (Bacchin et al. 2011). After the filtration in these systems, the PDMS microsystems are periodically rinsed with ultrapure deionized water.

2.2 Latex dispersion filtered in microseparators

The dispersion used in the present study consisted in monosized polystyrene microspheres (latex) [sulfate latex Invitrogen A37306]. The latex particle diameter was 4.90 ± 0.21 µm. The pore/particle size ratio is then 4. The latex suspensions used in the filtration experiments were obtained by diluting the concentrated latex suspension in aqueous solutions until the volume fraction reaches 5.10^{-3}. Aqueous solutions were ultrapure water or KCl solution (10^{-1} M in KCl) to reduce the magnitude of repulsive interactions between surfaces. This KCl concentration is lower than the critical salt concentration in a quiescent fluid (0.2 M) in order to avoid the aggregation of particles. Prior to experiments, the dispersion is exposed to ultrasonic waves during several seconds in order to avoid an aggregation of the latex particles.

2.3 Direct observation procedure

A constant suspension mean velocity ($V_{mean} = 0.0045$ ms^{-1}) in the larger upstream channel was imposed through the microseparators by a syringe pump feeding the latex dispersion (Sky Electronic PS 2000). The microseparator was placed on the stage of an Axiolab (Zeiss) microscope with a magnification of $\times 100$, see Fig. 2, and images were acquired using a high-sensitivity camera (Pixelfly QE, PCO). The exposure

time for the camera was 6.10^{-3} s, and the dynamic of the deposit formation was recorded by grabbing images every 20 s of filtration. The captured particle positions (for the very first layers of particles to deposit) and, later on, the cake of deposited particles were easily discernible on the images. As a particle displacement during the exposure time was several times its diameter, the resulting blur could be used to appreciate trajectories of individual particles near the entrance of the microchannels.

The image has been analyzed by the application of a thresholding technique (ImageJ software). It helps to quantify the surface occupied by the deposited particles present in the microsystem in the different part of the microseparator (inside the microchannels—internal clogging- or above the microchannels—superficial deposit). The binarization of the obtained images, facilitated by the strong contrast between the adhered particles and the rest of the microsystem image, allows the determination of the number of pixels occupied by the PDMS wall and deposited particles. The number of pixels corresponding to the first recorded image (image with microchannels only) has been subtracted from the pixel values of other images recorded in time in order to take into account the deposited particles. This normalized number of pixels is then converted to the surface (mm^2 in particular) due to the known dimensions for engravings present in the microsystem: 1 mm corresponds to 783 pixels.

2.4 Numerical model (Geodic software)

At pore scale, the exact description of the particle transport in a porous media is made difficult: the particles and pore sizes are of the same order of magnitude, and hydrodynamic interactions between the particle and the membrane have to be accounted for. The simulations have been made with the software GeoDict (Fraunhofer ITWM), which allows the calculation of the transport of particles in complex porous media. The created volume (Fig. 3) is a parallelepiped mesh in elementary cubes, called voxels, whose size is determined by the user. In our simulation, the voxel size corresponds to 0.45 µm. Each voxel is either a fluid element or a solid element (red voxels in Fig. 3). The boundary conditions for the simulations are inlet and outlet conditions in the opposite inlet and outlet surfaces and periodic conditions on others surfaces (Fig. 3). Different volumes have been created in order to mimic the microfluidic geometries (Fig. 1).

During the computation, the Navier–Stokes-Brinkman equations are solved (Wiegmann et al. 2009) to determine the fluid velocities. When inertial term can be neglected (the case of the present work), the system corresponds to Stokes equations with the conservation of momentum (Eq. 1) and mass (Eq. 2):

$$-\mu\Delta\vec{u} + \nabla p = \vec{f} \tag{1}$$

$$\nabla\vec{u} = 0 \tag{2}$$

with: $\vec{u}$, fluid velocity (ms^{-1}) μ, dynamic fluid viscosity (Pa s) p, pressure (Pa) $\vec{f}$, external forces applied on the fluid (N).

In the present case, the FFF-Stokes solver (Wiegmann et al. 2009) was used to solve these equations.

Once the velocity field is determined, the code determines particles trajectories. For the computation of the particles tracking, the trajectories of particles are solved in the fluid velocity field by applying the second Newton's law for each particles accounting for the drag force and the Brownian motion (described with a Wiener process):

$$\frac{d\vec{x}}{dt} = \vec{v} \tag{3}$$

$$\frac{d\vec{v}}{dt} = -\gamma(\vec{v}(\vec{x}(t)) - \vec{u}(\vec{x}(t))) + \sigma\frac{d\vec{W}(t)}{dt} \tag{4}$$

with, t, time (s); $\vec{x}$, position vector of particle (m); $\vec{v}$, particle velocity ($m.s^{-1}$); $\vec{u}$, fluid velocity ($m.s^{-1}$); $\vec{W}(t)$, Wiener process for Brownian diffusion force ($s^{-1/2}$).

The first term of Eq. 4 corresponds to the drag force. Its expression is valid for a Stokes flow ($10^{-4} < Re < 1$).

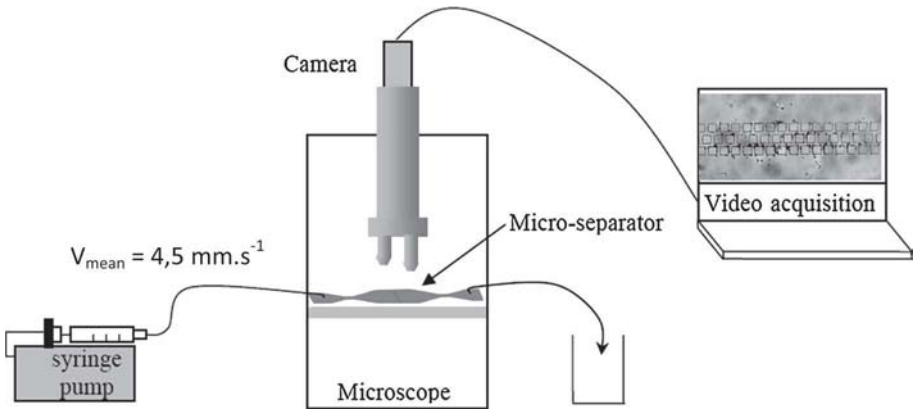

Fig. 2 Scheme of the experimental device

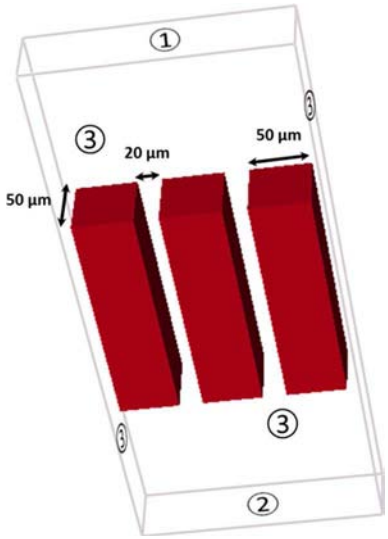

Fig. 3 Scheme of the model for numerical simulation (surface *1* inlet, surface *2* outlet, surfaces *3* periodic conditions)

Coefficient γ corresponds to the drag coefficient divided by the particulate mass:

$$\gamma = \frac{6\mu R}{m} \tag{5}$$

with R, particle radius (m); m, particle mass (kg).

The second term of Eq. 4 corresponds to the Brownian motion described by a Wiener process. The coefficient σ is given by Einstein's fluctuation–dissipation theorem:

$$\sigma^2 = \frac{2k_B T\gamma}{m} \tag{6}$$

with k_B, Boltzmann constant (J K^{-1}); T, Temperature (K).

When computing the particle trajectory, collision detection tests with walls are performed at each time step by comparing the particle position, its radius and the localization of the closest solid voxels. In case of particle–wall surface collision, there is a capture condition described by a balance between the kinetic energy of the particle and the Hamaker constant, the attractive interaction between the particle and the wall. In case of bounce, the restitution coefficient represents the rate of recovered energy, and when there is a capture, the particle cannot be detached. In standard simulations, the restitution coefficient for bounce is taken at 1 (theoretically, this coefficient is about 0.95 for an elastic plastic choc) and the Hamaker constant is 10^{-20} J: a standard value for the Van der Waals interactions between organic materials. In the present case, the repulsive interactions (Coulombian forces can be implemented in GeoDict) are not added as it cannot depict the physics of ionic repulsions (DLVO forces) occurring between colloids in water. By using this code, we assume that only attractive interaction (through the Hamaker constant) exists between the flowing particle and the walls.

A simulation contains several batches, whose number of sent particles and mean flux are fixed (here 0.0045 ms^{-1}). During a batch, all the particles start on the inlet surface. The position of the particles on the surface is determined randomly with a seed. Thus, with a same seed, the position of the particles is identical. In a batch, the flow velocity is determined by solving Eqs. 1, 2; therefore, the trajectories of particles are computed (Eqs. 3–6), and the capture of particles (if any) is determined. After these calculations, the captured particles are "aggregated" to the wall to form a new porous medium that will be used for the next batch calculation. Iterating these calculations for several batches allows to compute the permeability reduction due to particle capture within the porous media. In this paper, all the simulations have been realized with a monodispersed particle size (5 µm).

First simulations with such conditions show important discrepancies between the simulations results and the experiments in microfluidic devices. In simulations, there is a rapid capture of particles inside the microchannels or in the entrance corner of the microchannels leading to a rapid formation of arches. At the opposite, during experiments no permanent deposition is observed within straight pores; when a deposited particle is observed in the channels in one picture, in the next picture the particle is no longer at the same position. Experimentally, the deposited particles are then swept along by the strong velocity of the fluid in the microchannel. However, the re-suspension of particles by the flow cannot be accounted by GeoDict software. To overcome this problem, the wall in the microchannels (parallel to the fluid flow) has been considered as non-adherent by applying on these specific surfaces a Hamaker constant of zero and a restitution coefficient of 1.

3 Experiments on microseparators

The filtration conditions in microseparators have been chosen to be close to the ones of the microfiltration process. The velocity is equal to 4.5 mm s^{-1} in the large upstream channel and to 20.5 mm s^{-1} in the microchannels. The superficial filtration velocities (around 16 m h^{-1}) are in the range of those used in membrane microfiltration (up to 50 m h^{-1}, based on data for a MF-Millipore membrane with 8 µm pore size, operated at 100 mbar) and in conventional filtration with wooden filters or sand filters (up to 20 m h^{-1} for rapid filtration). So, the Reynolds number is, respectively, 0.44 and 0.58. The characteristic length used for the calculation of Reynolds number is here the channel hydraulic diameter. Regarding the inertial effects, the Stokes number is about 10^{-4}. Therefore, it is clear that the particles follow the streamlines (low inertial effects). The Peclet number is about 10^5, so the Brownian

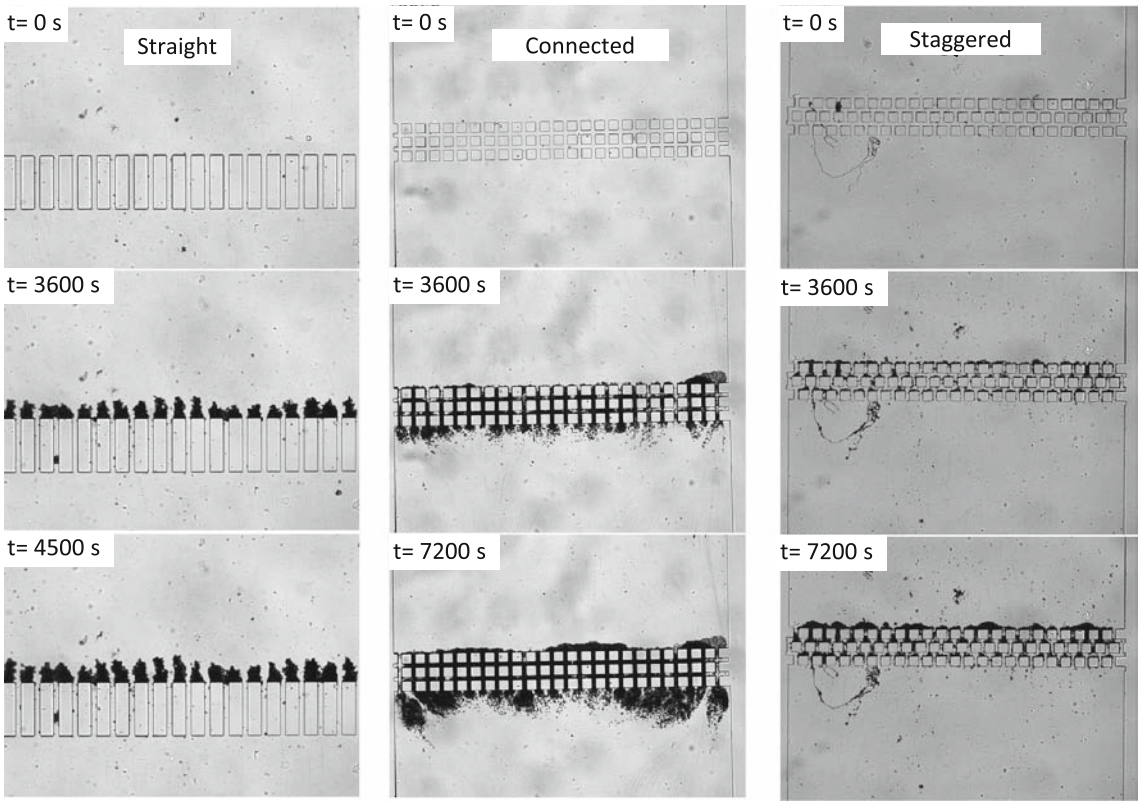

Fig. 4 Effect of microchannels geometry on the plugging. Images are taken at different times during the filtration (filtration velocity from the top to the bottom) of 5 μm latex particles with a volume fraction of 10^{-3}. The fluid velocity is 4.5 mm s^{-1}. Particles are dispersed in 10^{-1} M KCl solution

motion has a weak influence on the particles trajectory. Particle sedimentation can be neglected as the particle settling time (the settling velocity is O(1) μm/s) over the height of the microchannel (50 μm) was much larger than the particle residence time in a microchannel (10 ms). The next section presents the effect of the porous media geometry, of the ionic strength (playing on particle–wall surface interactions) and of fluid velocity on the clogging dynamics.

Preliminary experiments have been performed by varying the concentration in KCl in the solution where particles are dispersed. These first experiments have confirmed the importance of this parameter on the capture efficiency that has already been discussed (Agbangla et al. 2012). Only a few captures of particles are observed after 2 h of filtration when particles are dispersed in ultrapure water in all the geometries presented in this paper, whereas fouling is observed when processing with particles diluted in 10^{-1} M KCl solution (concentration chosen in order to reduce the magnitude of repulsion between particles without having particle aggregation). This trend can be explained by the existence of enhanced repulsive electrostatic interaction (higher magnitude and longer interaction range) in the absence of ions in the solution that prevents particle adhesion on PDMS walls.

3.1 Effect of tortuosity and connectivity of the porous geometry

Experiments performed with different geometries are presented in Fig. 4. The volume fraction of the dispersion is 10^{-3}, and the fluid velocity is 4.5 mm s^{-1} (around 42 million of particles are sent in 2 h). The particles are dispersed in 10^{-1} M in KCl in order to reduce the repulsion between particles and the wall. Different clogging modes can be observed.

When filtering in straight channels, the formation of dendrites on the wall at the upstream side is observed: the particles pile up on the top of the PDMS bar and do not clog the microchannels. After 75 min of filtration, the particles begin to clog the microchannels (the pores of this membrane) and the filtration efficiency also decreases. At this time, about 2.10^{14} particles have been sent in the microseparator (thus representing a volume of particles of $12.5.10^{-3}$ mL). A rough estimation of the volume of captured particles leads to estimate a maximum (a fifth of the

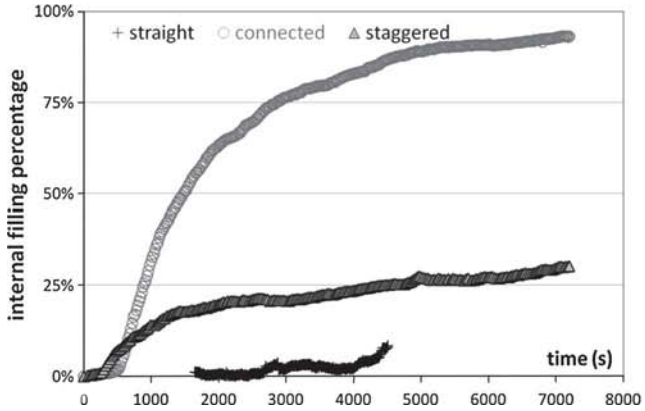

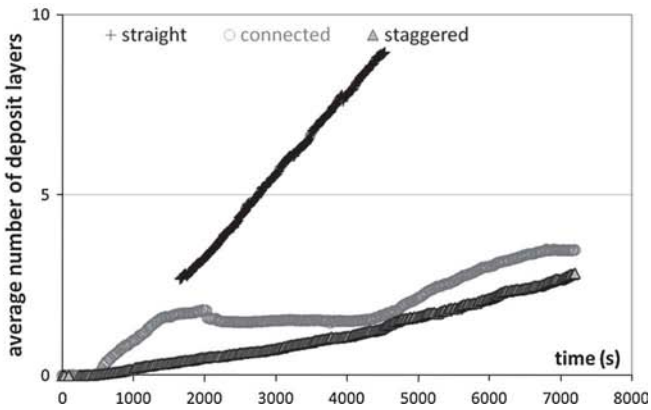

Fig. 5 Variation with time of the internal filling percentage (ratio of the surface occupied by particles over the total available surface within the porous media) and of the average number of deposit layers (ratio of the mean deposit thickness in the upstream zone over the particle size). In each figure, the variations are represented for the three different geometries: cross for straight channels, circle for connected channels and triangle for staggered rows

volume of the bars) of 2 10^{-6} mL ((20 × 200 μm × 50 μm × 50 μm)/5) of captured particles. The capture efficiency is then very low (<0.1 %).

With staggered pillars, particles are captured at first between the second and third rank, and then, the capture happens higher in the forest of square pillars. Later on, these particle accumulations lead to the blockage of the channels and to the formation of deposit on the upstream side. This filtration leads to a quicker clogging of channels than the one for straight channels. Contrary to the case of the parallel microchannels, there is no piling up on the pillars.

Similar behavior (internal pore blocking leading to deposit formation) is observed with aligned pillars geometry. A specific observation has been made with aligned pillars: the presence of an important deposit on the downstream zone is observed. This filtration leads to a quicker clogging of channels than the previous one: the filtration efficiency is higher. The origin of this deposit will be considered in the discussion section.

The dynamic of the clogging within the space inside the porous media (internal filling) and in the upstream zone (average number of deposit layers) is represented in Fig. 5.

The geometry with the aligned pillars (or connected pores) is quickly filled with the particles: almost 90 % of the internal porous void is darkened by the presence of particles. A rapid internal filling is observed for staggered pillars, whereas the internal filling stays to a very low level with straight channel. The formation of the superficial deposit (Fig. 5b) grows with almost the same velocity in the case of aligned or staggered pillars; in the case of the formation of the deposit, the layer is mainly due to pore blockage, which leads to the progression of the deposit in the upstream zone (deposit grows from the pore sections between the microchannel wall). The variation in superficial deposit is more important in the case of straight channel but the deposit formation has different characteristics here. The deposit here is due to the formation of dendrites on the microchannels walls between open sections. Some explanations for these different fouling structures will be given in the discussion section at the light of the simulation results.

3.2 Effect of the fluid velocity

Experiment (Fig. 6) has been conducted in the same conditions but with a more important velocity (9 mm s^{-1} in the large upstream channel and to 21 mm s^{-1} in the microchannels). When comparing experiments realized with different velocities (Figs. 4, 6), it can be clearly seen that the clogging of the porous media is faster at a higher fluid velocity. The deposit observed after 2 h of filtration with the 4.5 mm s^{-1} is obtained only after 15 min when the fluid velocity is twice. In order to have a fair comparison of the clogging kinetics, the variations of the internal filling and of the number of deposit layer are plotted in Fig. 7 as a function of the filtered volume of particle per filter area (being the product of the filtration time, the fluid velocity and the volume fraction of particles). In this representation, the dynamic of the internal filling is slightly more important for higher velocities, but here, the difference is not really significant. The difference is more pronounced when considering the number of deposit layers: the deposit layers increase significantly more rapidly for the higher velocity. The increase in the fluid velocity seems then to favor the plugging of microchannels. It is here an additional effect of the inherent increase due to the increase in the particle flux density. Similar observations have been made with straight channels by (Agbangla et al. 2012) who defined a critical flux density of particle yielding arches and deposits. Such a phenomenon could be explained by the theory used to

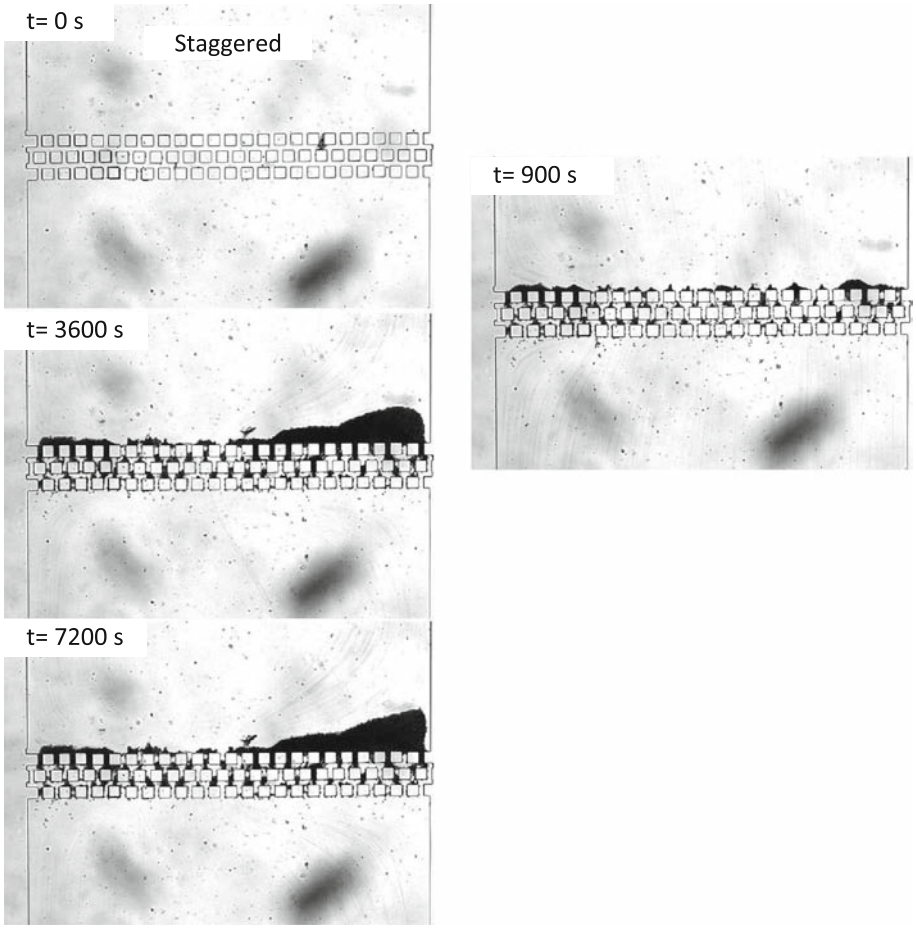

Fig. 6 Images taken for different filtration times of the clogging formation for a fluid velocity of 9 mm s^{-1} on staggered row pillars. These images have to be compared to the ones obtained in the same conditions but with a lower fluid velocity (4.5 mm s^{-1}) in Fig. 4. A similar deposit formation is observed at 900 s for a fluid velocity of 9 mm s^{-1} and at 7,200 s for a fluid velocity of 4.5 mm s^{-1}

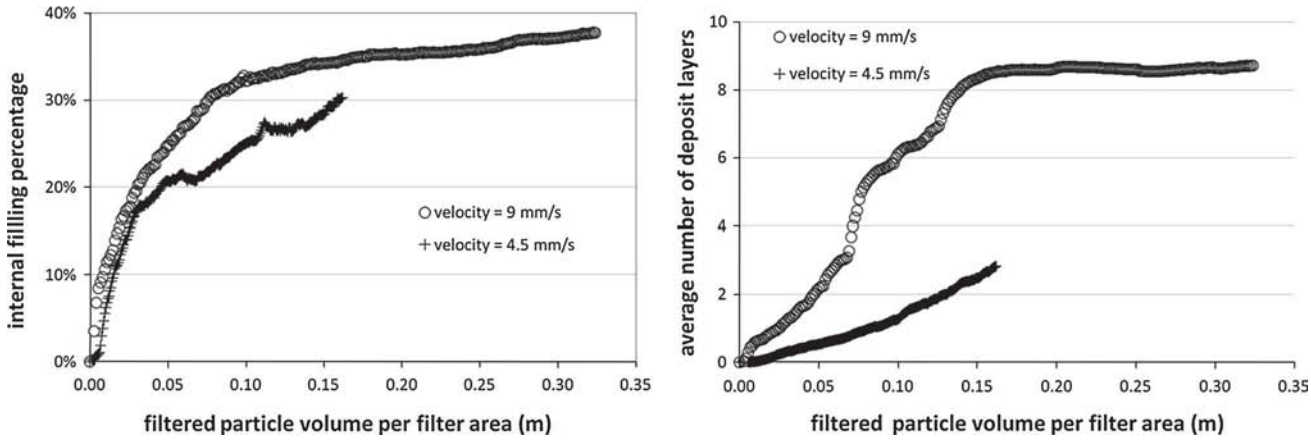

Fig. 7 Variation of the internal filling and of the number of deposit layers as a function of the volume of filtered particles per filter area (the product of the filtration time, the fluid velocity and the volume fraction of the dispersion) for a fluid velocity of 4.5 and 9 mm s^{-1}

define critical flux (Bacchin et al. 2006a) and critical filtered volume (Bessiere et al. 2005) concepts in filtration where a critical flux (or a critical filtered volume) has been defined above which the drag force on particles near the porous surface is important enough to overcome particle–wall interactions and leads to the formation of deposit.

Additionally, it can be note with the experiment at 9 mm s^{-1} that the deposit formation seems to reach a stability zone after 1 h (Fig. 7b). This plateau seems to be due to the tangential velocity acting on the top of the deposit: streamlines of particles parallel to the deposit surface can be seen above the dense deposit in the right part

of the image after 1 or hours (Fig. 6). Such tangential velocity prevents the growing of the cake because of a sweeping effect as it is classically observed with cross-flow filtration. Our experiments are operated in a dead end filtration mode (one inlet and one outlet) but the non-homogeneity in the deposit formation and by consequence in the fluid distribution through the microchannels induces local tangential velocities that prevent further deposit formation.

4 Numerical simulations

Numerical simulations have been performed with GeoDict software in order to analyze the particle capture in the porous geometries. Simulation parameters (velocity, geometrical structures, etc) have been chosen to correspond to the experiments. Simulations have been performed for 30,000 particles shared out in 30 batches corresponding to an experimental filtration time of 40 s.

The results of simulation with these conditions are presented in Figs. 8, 9 and 10 for the different geometries used during filtration experiments. For all the different geometries, the dynamic of capture is more important with simulations than with experiments: a formation of dense deposit at the entrance of the straight channels is observed after 40 s of simulation. The structure of deposited particles does not show the formation of dendrites (as it has been observed in experiments) but the formation of arches leading to dense deposit formation. In the staggered geometry (Fig. 10), important internal captures of particles are simulated: these clogging structures are close to the ones observed in the experiment. For connected microchannels (Fig. 9), it is an intermediate behavior with some

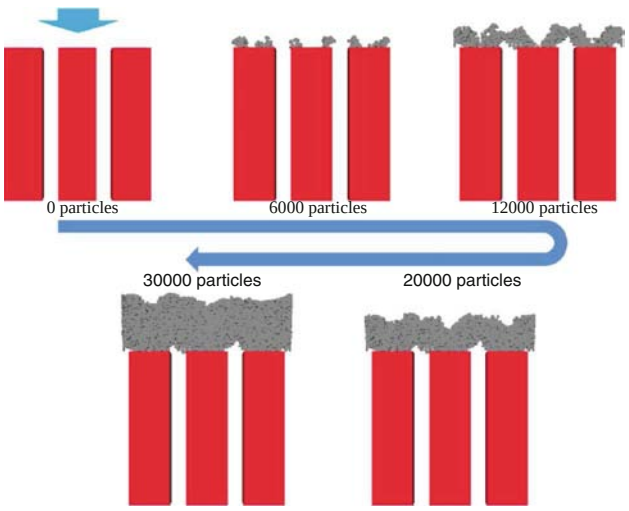

Fig. 8 Simulation of the capture of particles in straight channel geometry

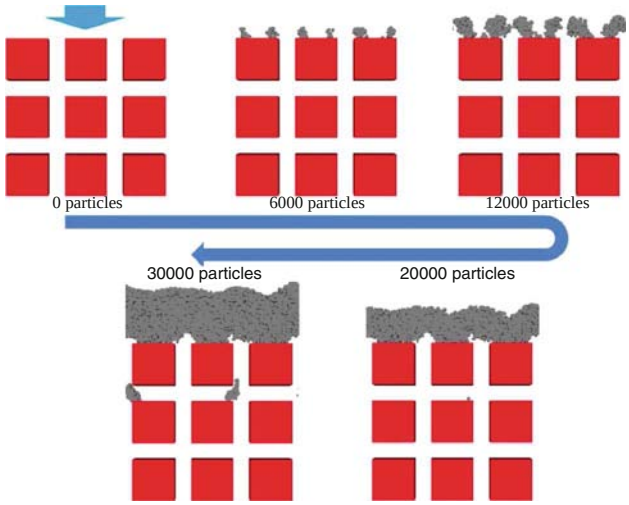

Fig. 9 Simulation of the capture of particles in connected channel geometry

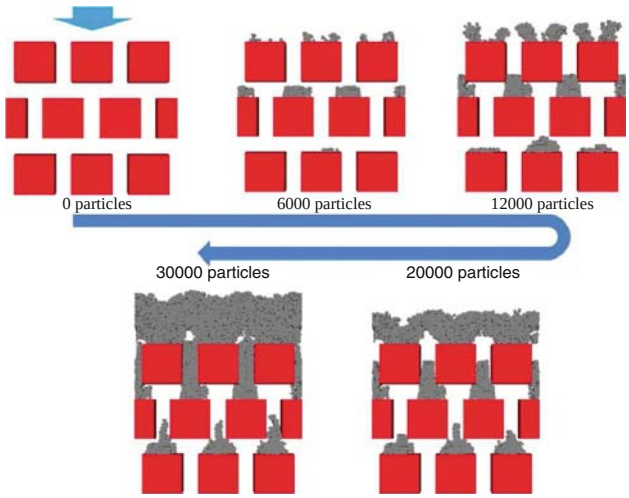

Fig. 10 Simulation of the capture of particles in staggered pillars geometry

internal deposit formation: as it will be discussed later in the paper, this internal clogging is due to the disturbance of fluid distribution within the pores.

The average capture efficiency is presented in Fig. 11 for the three simulations as a function of the number of filtered particles. This number is proportional to the simulation time. For all cases, the capture increases with time: the capture of particles enhances the probability to have a new capture site. Since the first time of simulation, the dynamic of the capture is faster with staggered pillars geometries. The formation of an internal deposit leads to have an important capture efficiency (more than 50 % after 30,000 particles sent). The capture efficiencies are very close for straight and connected channels. For connected channels, the efficiency is slightly lower at the beginning of the simulation and higher at the end of the simulation (probably because of the formation of

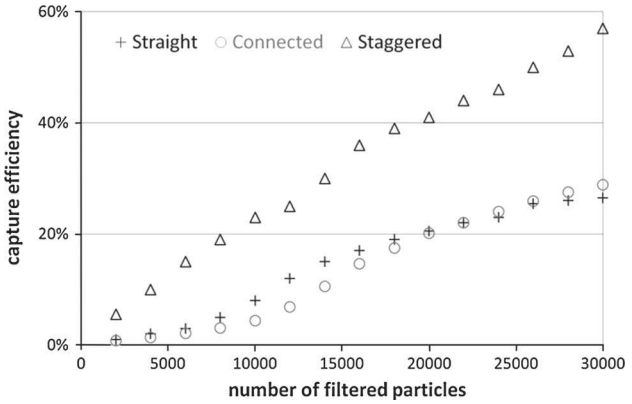

Fig. 11 Evolution of the capture efficiency as a function of the number of particles filtered through the geometries with straight channel, connected channels or staggered pillars (30,000 filtered particles correspond to 40 s of filtration during experiments)

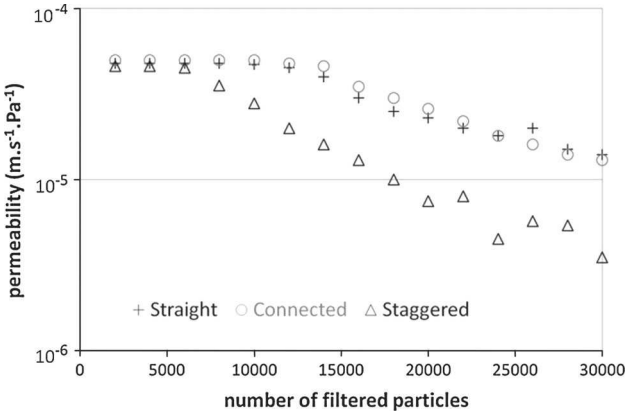

Fig. 12 Evolution of the permeability as a function of the number of particles filtered through the geometries with straight channel, connected channels or staggered pillars (30,000 filtered particles correspond to 40 s of filtration during experiments)

internal capture). When the evolution of the permeability is analyzed (Fig. 12), we can note for all geometries that the reduction in permeability is not significant at the beginning of the simulation, i.e., when initial particle capture on the wall does not reduce the permeability. When comparing the clogging for the different geometries, the same trends can be observed with a more pronounced reduction in permeability for the staggered pillars geometry; the permeability of the system at the end of simulation is only 5 % of the initial permeability. For the straight and connected channels, the reduction in permeability is of 40 % at the end of the simulation.

5 Discussion

Experiments and simulations presented in previous sections show the role of connectivity and tortuosity on the plugging of microchannels. For all geometries, the simulations allow the reproduction of the behavior observed qualitatively with an internal clogging and the formation of dense deposit. However, simulations do not allow a good depicting of the capture kinetics: in simulations, a cake layer is obtained in less than one minute (a dense deposit is formed after the filtration of 30,000 particles corresponding to 40 s filtration duration as seen in Fig. 8), whereas in the same conditions, several hours are needed during experiments (a ten layer deposit is obtained after 1 or 2 h of filtration as seen in Fig. 5). The time constant is then not recovered properly in the simulations: the kinetic is overestimated in simulations by a factor between 100 and 1,000. Such a discrepancy can be due to the overestimation of the capture efficiency in simulations. As discussed in Sects. 2–4, the capture condition used in Geodict is based on a balance between the particle kinetic energy and the Hamaker constant and then does not account for repulsive surface interactions. It is well known that the capture kinetics is controlled by surface interactions for small particles in porous media (Elimelech and O'Melia 1990) or within microchannels (Chatterjee et al. 2012). It has been demonstrated (Verwey and Overbeek 1948) that the aggregation constant in presence of repulsive surface interaction (reaction-limited aggregation or slow aggregation) is inversely proportional to the colloidal stability ratio (playing the role of the inverse of the capture efficiency). A stability ratio between 100 and 1,000 could then explain the difference of kinetics between simulations and experiments. Such stability ratio corresponds to weak potential barrier (between 10 and 20 k_BT) that can be possibly encountered between micrometric particles dispersed in 10^{-1} M in KCl (the repulsive interaction is not totally screened by the salt: the critical concentration for coagulation has been measured at 2 10^{-1} M in KCl). The presence of weak repulsive colloidal interactions (not accounted in the simulation) could explain why faster clogging kinetics are obtained with simulations.

In straight channels, during filtration on microseparators, particles do not accumulate within the microchannels (particles are swept away by the fluid velocity) but pile up on pillars to form dendrites (Fig. 4a) or for higher fluid velocities to form arches leading to dense deposit formation (Fig. 6). Simulations with GeoDict software by considering non-adherent surface inside the pores can describe such arches and dense deposit formations in several steps. Initially, particles on critical hydrodynamic trajectories are captured at the entrance channel corners (such an initial particle deposition at a pore corner has already been observed and discussed by Lin et al. 2009). Then, particles accumulate in the upstream zone of these first deposited particles or laterally to these particles to form dendrites at the corner of the channel (as seen after 6,000 particles in Fig. 8).

In a third step, such deposits can join to form arches at the pore entrance (after 12,000 particles in Fig. 8). Finally, it leads to a cake layer formation in the upstream zone of the filtration area (after 30,000 particles in Fig. 8). These observations are also in agreement with simulations already performed (Ando et al. 2012). For the same pore/particle size ratio of 2.5, these authors show a fouling mode in which particles are accumulated on the surface of the membrane without filling the pores and in which a cake layer forms across the entire filtration area.

When adding tortuosity in the porous media with staggered pillars geometry, in experiments and in simulation, particles start to be captured in the porous media primarily on the surface perpendicular to the main fluid direction. This accumulation occurs both on the different layers of the porous media. The volume occupied by these accumulations increases with time and goes back up to the pore entrance. It leads with time to a pore blockage that induces, later on, the growth of a cake layer in the upstream zone. The tortuosity in the porous media plays then an important role in the internal blocking of particles leading to the clogging of the system.

When adding connectivity in the porous media with connected microchannels, at the beginning the clogging behavior is very similar to the clogging observed with straight channels. However, with time and because of the first particle capture, the flow distribution is no longer homogeneous and induces flow velocities in the connection zone between channels (Fig. 13). This deviation of the streamlines through the porous media enhances the internal deposition of particles, as it has been observed in a more pronounced way and since the beginning of experiments or simulation with the tortuous porous media. The nonuniform flow distribution in connected channels induces local changes in fluid velocity and even in the flow direction. These streamline changes seem to be responsible for the detachment and transport of particle aggregate through the network which settles in the dead end zone existing in the porous media because of the connection between pores: the settling velocity of a particle is in the range of micrometers per second, and then, about 10 s in a stagnation point is sufficient for a particle to settle along the height of the microchannels. The settling leads to the deposition of particle cluster in the porous media and in the downstream zone. In the connected geometry, the interplay between these phenomena leads to the particular clogging pattern observed during experiments (Fig. 4b). The formation of aggregate in these connected microchannels could then be controlled by aggregate–aggregate interactions. Such a behavior has been put in evidence by (Gudipaty et al. 2011; Stamm et al. 2011) during the study of cluster growth kinetics: they show the important role of constructive and destructive cluster–cluster interactions on the aggregation process in microchannels. These phenomena are rather complex and cannot be fully simulated with GeoDict software: the particle detachment and re-entrainment by the fluid as well as the settling are not accounted for.

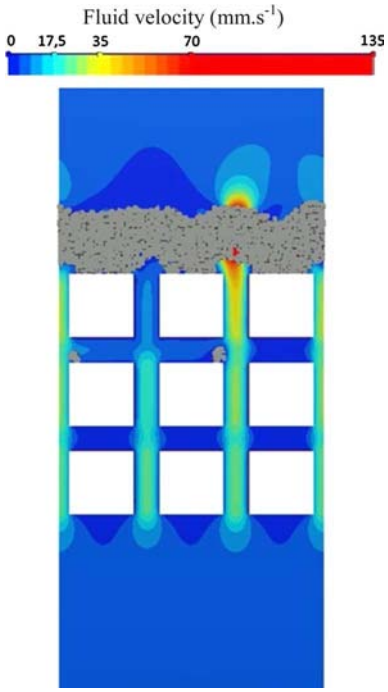

Fig. 13 Illustration of the distribution of flow through the connected channels encountered during simulation. Some connections between channels are swept by fluid velocities, whereas other connections correspond to dead end zone. This flow distribution enhances the particle deposition in the connection because of "fluid tortuosity" through the porous media. Such a phenomenon can also be at the origin of the detachment of the deposited aggregates because of transient change in fluid distribution and to the settling of aggregates when the connection is not swept away by fluid–dead flow zone

6 Conclusions

Micronic particle filtration in microfluidic devices has been realized with three kinds of microchannels geometries: straight microchannels, connected microchannels (or aligned square pillars) and staggered square pillars. The direct observation of the clogging phenomena in these devices has been analyzed at the light of simulations of the particle capture in such geometries with GeoDict software. These results allow determining the effect of tortuosity and connectivity on the clogging of porous media. With straight parallel channels at high velocity, the clogging is the consequence of arches formation at the channel entrance leading to cake formation. For lower fluid velocity, only dendrites (accumulation on pillars) are observed. With a tortuous porous media (staggered pillars), a progressive plugging of the internal spaces occurs, and, later on, the

plugging progresses toward the upstream zone and leads to the blocking of the channels entrance and to the formation of a dense superficial deposit. For connected channels, an intermediate clogging behavior is observed. Because of the initial capture of particles at the pore entrance, the distribution of the flow inside the channels is modified, and then, the dead connection zone between pores can be flowed. The deviation of streamline toward the connection zone can then lead to the capture of particles inside the porous media as it has been observed with tortuous porous media. These behaviors are simulated with GeoDict software with a good qualitative agreement. The different steps leading to the formation of the deposit can then be identified. However, a quantitative description of the clogging dynamic of the clogging was not possible mainly because colloidal interaction and particle re-entrainment cannot be accounted for in simulations.

Acknowledgments The authors would like to thank Dr. Andréas Wiegmann for the helpful discussions on GeoDict software and Dr. Aurélie Marty for her help in the experimentation part. Dr. Paul Duru is thanked for his help in the conception and the elaboration of microseparators. This work was funded by Suez Environnement group.

References

Agbangla GC, Climent E, Bacchin P (2012) Experimental investigation of pore clogging by microparticles: evidence for a critical flux density of particle yielding arches and deposits. Sep Purif Technol 101:42–48

Ando T, Akamatsu K, Nakao S, Fujita M (2012) Simulation of fouling and backwash dynamics in dead-end microfiltration: effect of pore size. J Membr Sci 392–393:48–57

Bacchin P, Aimar P, Field RW (2006a) Critical and sustainable fluxes: theory, experiments and applications. J Membr Sci 281:42–69

Bacchin P, Espinasse B, Bessiere Y, Fletcher DF, Aimar P (2006b) Numerical simulation of colloidal dispersion filtration: description of critical flux and comparison with experimental results. Desalination 192:74–81

Bacchin P, Marty A, Duru P, Meireles M, Aimar P (2011) Colloidal surface interactions and membrane fouling: investigations at pore scale. Adv Colloid Interface Sci 164:2–11

Bessiere Y, Abidine N, Bacchin P (2005) Low fouling conditions in dead-end filtration: evidence for a critical filtered volume and interpretation using critical osmotic pressure. J Membr Sci 264:37–47

Bowen WR, Filippov AN, Sharif AO, Starov VM (1999) A model of the interaction between a charged particle and a pore in a charged membrane surface. Adv Colloid Interface Sci 81:35–72

Bromley A, Holdich R, Cumming I (2002) Particulate fouling of surface microfilters with slotted and circular pore geometry. J Membr Sci 196:27–37

Chandler M, Zydney A (2006) Effects of membrane pore geometry on fouling behavior during yeast cell microfiltration. J Membr Sci 285:334–341

Chatterjee R, Bhattacharjee S, Mitra SK (2012) Particle transport in patterned cylindrical microchannels. Microfluid Nanofluid 12:41–51

Chen JC, Li Q, Elimelech M (2004) In situ monitoring techniques for concentration polarization and fouling phenomena in membrane filtration. Adv Colloid Interface Sci 107:83–108

Elimelech M, O'Melia CR (1990) Kinetics of deposition of colloidal particles in porous media. Environ Sci Technol 24:1528–1536

Grenier A, Meireles M, Aimar P, Carvin P (2008) Analysing flux decline in dead-end filtration. Chem Eng Res Des 86:1281–1293

Gudipaty T, Stamm MT, Cheung LSL, Jiang L, Zohar Y (2011) Cluster formation and growth in microchannel flow of dilute particle suspensions. Microfluid Nanofluid 10:661–669

Henry C, Minier J-P, Lefèvre G (2012) Towards a description of particulate fouling: from single particle deposition to clogging. Adv Colloid Interface Sci 185–186:34–76

Hermia J (1982) Constant pressure blocking filtration law application to powder-law non-Newtonian fluid. Trans Inst Chem Eng 60:183–187

Kim M, Zydney AL (2004) Effect of electrostatic, hydrodynamic, and Brownian forces on particle trajectories and sieving in normal flow filtration. J Colloid Interface Sci 269:425–431

Kuiper S, van Rijn CJ, Nijdam W, Krijnen GJ, Elwenspoek M (2000) Determination of particle-release conditions in microfiltration: a simple single-particle model tested on a model membrane. J Membr Sci 180:15–28

Lin J, Bourrier D, Dilhan M, Duru P (2009) Particle deposition onto a microsieve. Phys Fluids 21:073301–0733014

McDonald JC, Duffy DC, Anderson JR, Chiu DT, Wu H, Schueller OJA, Whitesides GM (2000) Fabrication of microfluidic systems in poly(dimethylsiloxane). Electrophoresis 21:27–40

Mustin B, Stoeber B (2010) Deposition of particles from polydisperse suspensions in microfluidic systems. Microfluid Nanofluid 9:905–913

Ramachandran V, Fogler HS (1998) Multilayer deposition of stable colloidal particles during flow within cylindrical pores. Langmuir 14:4435–4444

Ramachandran V, Fogler HS (1999) Plugging by hydrodynamic bridging during flow of stable colloidal particles within cylindrical pores. J Fluid Mech 385:129–156

Sharp KV, Adrian RJ (2005) On flow-blocking particle structures in microtubes. Microfluid Nanofluid 1(4):376–380

Stamm MT, Gudipaty T, Rush C, Jiang L, Zohar Y (2011) Particle aggregation rate in a microchannel due to a dilute suspension flow. Microfluid Nanofluid 11:395–403

Verwey EJW, Overbeek JTG (1948) Theory of the stability of lyophobic colloids. Courier Dover Publications

Wiegmann A, Rief S, Latz A, Iliev O (2009) Toward predicting filtration and separation : progress and Challenges. Filtech, Wiesbaden, Deutschland 1:48–63

Wyss HM, Blair DL, Morris JF, Stone HA, Weitz DA (2006) Mechanism for clogging of microchannels. Phys Rev E 74:061402